

Length sensing and control of a Michelson interferometer with Power Recycling and Twin Signal Recycling cavities

Christian Gräf, André Thüring, Henning Vahlbruch,
Karsten Danzmann and Roman Schnabel

*Institut für Gravitationsphysik, Leibniz Universität Hannover and Max-Planck-Institut für
Gravitationsphysik (Albert-Einstein Institut), Callinstrasse 38, 30167 Hannover, Germany*

christian.graef@aei.mpg.de

Abstract: The techniques of power recycling and signal recycling have proven as key concepts to increase the sensitivity of large-scale gravitational wave detectors by independent resonant enhancement of light power and signal sidebands within the interferometer. Developing the latter concept further, *twin signal recycling* was proposed as an alternative to conventional detuned signal recycling. Twin signal recycling features the narrow-band sensitivity gain of conventional detuned signal recycling but furthermore facilitates the injection of squeezed states of light, increases the detector sensitivity over a wide frequency band and requires a less complex detection scheme for optimal signal readout. These benefits come at the expense of an additional recycling mirror, thus increasing the number of degrees of freedom in the interferometer which need to be controlled.

In this article we describe the development of a length sensing and control scheme and its successful application to a tabletop-scale power recycled Michelson interferometer with twin signal recycling. We were able to lock the interferometer in all relevant longitudinal degrees of freedom, enabling the long-term stable operation of the experiment. We thus laid the foundation for further investigations of this interferometer topology to evaluate its viability for the application in gravitational wave detectors.

© 2012 Optical Society of America

OCIS codes: (120.2230) Fabry-Perot, (120.3180) Interferometry, (120.3940) Metrology, (120.4640) Optical instruments, (120.4820) Optical systems, (230.4555) Coupled resonators.

References and links

1. B. Willke for the GEO collaboration, "The GEO-HF project," *Class. Quantum Grav.* **23**, S207–S214 (2006).
2. G. M. Harry for the LIGO scientific collaborations, "Advanced LIGO: the next generation of gravitational wave detectors," *Class. Quantum Grav.* **27**, 084006 (2010).
3. The Virgo collaboration, "Status of the Virgo project," *Class. Quantum Grav.* **28**, 114002 (2011).
4. K. Somiya for the KAGRA collaboration, "Detector configuration of KAGRA – the Japanese cryogenic gravitational-wave detector," *Class. Quantum Grav.* **29**, 124007 (2012).
5. B. J. Meers, "Recycling in laser-interferometric gravitational-wave detectors," *Phys. Rev. D* **38**, 2317–2326 (1988).
6. S. Hild, H. Grote, M. Hewitson, H. Lück, J. R. Smith, K. A. Strain, B. Willke, and K. Danzmann, "Demonstration and comparison of tuned and detuned signal recycling in a large-scale gravitational wave detector," *Class. Quantum Grav.* **24**, 1513–1523 (2007).

7. C. M. Caves, “Quantum-mechanical noise in an interferometer,” *Phys. Rev. D* **23**, 1693–1708 (1981).
 8. R. Schnabel for the LIGO scientific collaboration, “A gravitational wave observatory operating beyond the quantum shot-noise limit,” *Nature Physics* **7**, 962–965 (2011).
 9. J. Harms, Y. Chen, S. Chelkowski, A. Franzen, H. Vahlbruch, K. Danzmann, and R. Schnabel, “Squeezed-input, optical-spring, signal-recycled gravitational-wave detectors,” *Phys. Rev. D* **68**, 042001 (2003).
 10. H. J. Kimble, Y. Levin, A. B. Matsko, K. S. Thorne, and S. P. Vyatchanin, “Conversion of conventional gravitational-wave interferometers into quantum nondemolition interferometers by modifying their input and/or output optics,” *Phys. Rev. D* **65**, 022002 (2002).
 11. A. Thüring, R. Schnabel, H. Lück, and K. Danzmann, “Detuned twin signal recycling for ultra-high precision interferometers,” *Opt. Lett.* **32**, 985 (2007).
 12. A. Thüring, C. Gräf, H. Vahlbruch, M. Mehmet, K. Danzmann, and R. Schnabel “Broadband squeezing of quantum noise in a Michelson interferometer with Twin-Signal-Recycling,” *Opt. Lett.* **34**, 824 (2009).
 13. H. Vahlbruch, S. Chelkowski, B. Hage, A. Franzen, K. Danzmann, and R. Schnabel, “Demonstration of a squeezed-light-enhanced Power- and Signal-Recycled Michelson interferometer,” *Phys. Rev. Lett.* **95**, 211102 (2005).
 14. A. Freise, G. Heinzel, H. Lück, R. Schilling, B. Willke, and K. Danzmann, “Frequency-domain interferometer simulation with higher-order spatial modes,” *Class. Quantum Grav.* **21**, 1067 (2004).
 15. K. A. Strain, G. Müller, T. Delker, D. H. Reitze, D. B. Tanner, J. E. Mason, P. A. Willems, D. A. Shaddock, M. B. Gray, C. Mow-Lowry, and D. E. McClelland “Sensing and control in dual-recycling laser interferometer gravitational-wave detectors,” *Appl. Opt.* **42**, 1244 (2003).
 16. M. W. Regehr, F. J. Raab, and S. E. Whitcomb, “Demonstration of a power-recycled Michelson interferometer with Fabry-Perot arms by frontal modulation,” *Opt. Lett.* **20**, 1507 (1995).
 17. R. W. P. Drever, J. L. Hall, F. V. Kowalski, J. Hough, G. M. Ford, A. J. Munley, and H. Ward “Laser Phase and Frequency Stabilization Using an Optical Resonator,” *Appl. Phys. B* **31**, 97–105 (1983).
 18. J. Mizuno, “Comparison of optical configurations for laser-interferometric gravitational-wave detectors,” PhD Thesis, (Universität Hannover, 1995).
 19. M. Punturo et al. “The Einstein Telescope: a third-generation gravitational wave observatory,” *Class. Quantum Grav.* **27**, 194002 (2010).
-

1. Introduction

The international network of large-scale interferometric gravitational wave (GW) detectors is currently undergoing an extensive technological upgrade towards what is commonly referred to as the “second generation” of GW detectors. Upon completion, these second generation observatories, namely GEO-HF [1], Advanced LIGO [2] and Advanced Virgo [3], complemented by the new observatory KAGRA [4], will reach unprecedented sensitivities to GW-induced strain. This sensitivity improvement constitutes a major leap towards reaching the long-standing goal of the first direct measurement of GWs.

Besides power recycling (PR), which was already implemented in the first generation LIGO and Virgo interferometers, signal recycling [5] (SR) has been adopted for the optical layouts of all second generation detectors. Dual recycling, i.e. the combination of PR and SR, has already been successfully implemented and operated in the GEO 600 detector [6].

Furthermore, the injection of squeezed vacuum – a technique proposed by Caves to improve the quantum noise limited sensitivity of GW detectors [7] – will be employed to enhance the performance of GEO-HF as well as the Advanced LIGO Hanford observatory. The current GEO 600 detector has been the first large-scale interferometer to successfully demonstrate long-term stable squeezing injection and the associated broadband sensitivity improvement, already for the case of carrier-tuned SR. [8]

The compatibility of *detuned* SR interferometers with squeezing injection was investigated theoretically by Harms et al. [9]. This work led to the insight that the combination of these two techniques requires additional filter cavities in the squeezing path to take full advantage of the benefit from squeezing injection on the detector sensitivity. The use of filter cavities was previously suggested by Kimble et al. to compensate for radiation pressure noise in GW detectors [10].

As an alternative to conventional detuned SR, Thüring et al. proposed the technique of twin

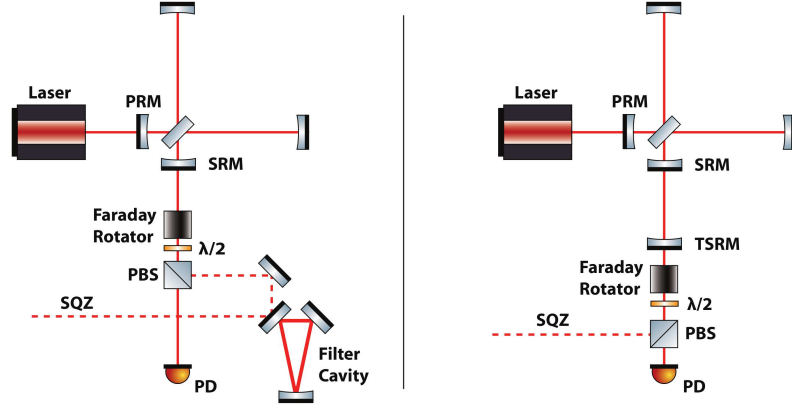


Fig. 1. General comparison of the dual recycling (left) and the power recycled twin signal recycling Michelson (right) topologies, both including squeezed light injection. Compared to dual recycling, the power recycled TSR interferometer features a second recycling mirror in the detection port, TSRM, which forms a three mirror coupled cavity together with the SRM and the Michelson end mirrors. For a broadband sensitivity improvement at shot noise limited frequencies by squeezing injection, the dual recycling interferometer with detuned SR requires an additional filter cavity, to compensate for the SR cavity-induced rotation of the squeezing ellipse. Contrasting this, the TSR topology is inherently compatible with squeezing at shot noise limited frequencies and requires no additional optical filter in the squeezing path.

signal recycling [11] (TSR) which is based on introducing a second recycling mirror in the asymmetric port of the interferometer (cf. Fig. 1). It was shown that, in contrast to detuned SR, an interferometer featuring TSR does not require additional filter cavities to maximize the benefit from squeezing injection in the shot noise-limited frequency regime. Besides this, Thüring points out further advantages of TSR over conventional detuned SR in his paper: a sensitivity improvement over a wide frequency band and a less challenging GW signal readout scheme. The former can be attributed to the simultaneous resonant enhancement of both the upper and the lower GW signal sidebands, which can be arranged for in TSR configurations. The latter stems from the fact that in TSR configurations the GW signal is entirely contained in the phase quadrature of the carrier field, similar to the case of a conventional Michelson interferometer.

In this paper we describe the electronic stabilization and long-term operation of a power recycled Michelson interferometer with TSR, thus laying the foundation for further investigations of this topology to evaluate its viability for the application in GW interferometry. One such aspect, the broadband enhancement of the interferometer by squeezed light injection, was carried out in a subsequent experiment and was already reported on in [12].

2. Layout of the power recycled TSR interferometer

The starting point of our investigations was an existing dual recycling Michelson interferometer (DRMI) tabletop experiment [13] – a scaled and largely simplified model of the GEO 600 interferometer – which we were aiming to extend to a power recycled TSR interferometer with a minimum of invasive changes. Thus, we were able not only to experimentally test the power recycled TSR topology but also to evaluate the viability of TSR as an upgrade for existing interferometers with conventional SR.

2.1. TSR cavity parameters

By introducing an additional recycling mirror into the optical setup of the DRMI, the former signal recycling cavity (SRC) is converted into a system of two optically coupled cavities which we refer to as the *twin signal recycling cavity* (TSRC) throughout this paper. This cavity is formed by the newly introduced mirror and the Michelson mirrors acting as the end mirrors, and the former signal recycling mirror acting as the coupling mirror. For clarity we will keep referring to the former signal recycling mirror as SRM and denote the newly introduced mirror as *twin signal recycling mirror* (TSRM). We will refer to the length of the TSRM–SRM cavity as L_{SR1} and, correspondingly, the average length of the cavity formed by the SRM and the Michelson end mirrors (i.e. the former SRC) will be denoted as L_{SR2} , in accordance with the nomenclature used in [11].

Three free parameters of the TSRM were to be determined: (i) reflectivity, (ii) radius of curvature (ROC) and (iii) distance to the SRM. These, either directly or indirectly, affect the frequency response as well as the structure of the sensing matrix of the “optical plant” which determines the complexity of the longitudinal control scheme.

The reflectivity of the TSRM influences the level of resonant enhancement of the signal sidebands, which is in close analogy to the role of the SRM reflectivity in a signal recycled interferometer. We chose a reflectivity of $R_{\text{TSRM}} = 95\%$ for our experiment.

The ROC of the TSRM and its distance to the SRM can, generally, not be chosen independently. The boundary conditions for a stable and (theoretically) well mode matched cavity constrain the values these parameters can reasonably take on. From the control point of view it was desirable to chose L_{SR1} such that, for given phase modulation (PM) control sideband frequencies, an error signal could be extracted for feedback to the TSRM which preferably exhibits only small coupling to the other longitudinal degrees of freedom (DOF) in the interferometer. For a known length L_{SR1} the corresponding TSRM curvature, which results in a stable and mode matched cavity, can then be easily determined. We will discuss our approach of determining the optimal length L_{SR1} , driven by control considerations, in the following section.

2.2. Development of a sensing scheme

For the design of the sensing scheme we performed a series of numerical simulations, based on a steady-state frequency domain model of the power recycled TSR interferometer realized with the software *Finesse* [14]. Besides the length L_{SR1} the optimal locations of the length signal extration ports to obtain error signals for the four longitudinal DOF of the interferometer were to be determined with the aid of the numerical model. These DOF are the differential mode of the Michelson arms (MICH), the power recycling cavity (PRC) and the microscopic positions of the TSRM relative to the SRM (δL_{SR1}) and the SRM relative to the average position of the Michelson end mirrors (δL_{SR2}), respectively.

Due to the coupled nature of the longitudinal DOF in a power recycled TSR interferometer the extracted heterodyne length signals, likewise, are coupled. This coupling can often be reduced by prudently designing the optical plant and the sensing system. However, the RF modulation scheme was carried over from the precursor DRMI experiment and modulation frequencies were thus not intended as free parameters for the optimization of the sensing scheme. As a consequence, the resulting sensing matrices were non-orthogonal but could be arranged for to have at least full rank by choosing appropriate values for the remaining free parameters. In this case the technique of *gain hierarchy* [15] can often be applied and was successfully used in earlier interferometry experiments, e.g. in [16].

To facilitate lock acquisition of the interferometer, polarization dependent sensing was employed to decouple length signals of coupled DOF. In this approach the polarization of the input beam is chosen to be a linear combination of s- and p-polarized light. A polarizing beam splitter

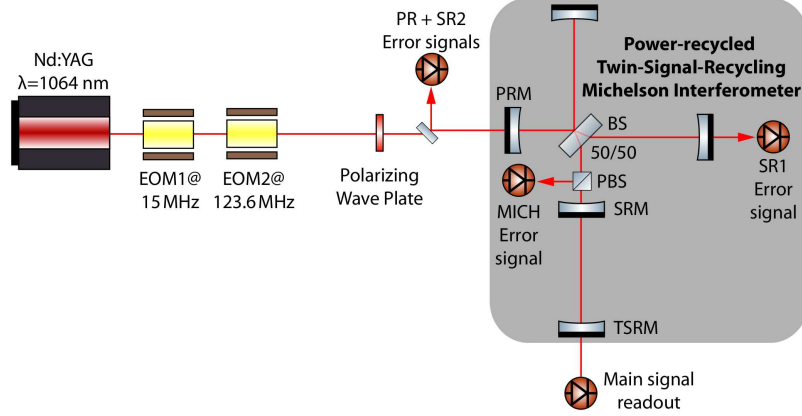


Fig. 2. Schematic drawing of the conceptual approach to length sensing in the TSR interferometer. The sensing scheme is based on two different pairs of phase modulation sidebands and four heterodyne signal extraction ports to obtain four error signals for feedback control of the longitudinal DOF of the interferometer. The wave plate in the input beam path and the polarizing beam splitter between the Michelson beam splitter and the SRM permit interferometer locking with orthogonal polarization modes.

Table 1. Modulation/demodulation parameters of the signal extraction system. In the first column the longitudinal DOF are listed along with, in brackets, the mirrors which were actuated upon to tune the respective DOF.

DOF (Mirror)	f_{demod}	ϕ_{demod}	Detection port
PRC (PRM)	15 MHz	in-phase	PRC reflected beam
MICH (EMx)	123.6 MHz	quadrature	internal pick-off (p-pol)
δL_{SR1} (TSRM)	123.6 MHz	in-phase	MI end mirror trans. beam
δL_{SR2} (SRM)	123.6 MHz	in-phase	PRC reflected beam

between the Michelson beam splitter and the SRM serves to separate s-polarized light, which circulates in the TSRC, from p-polarized light, which exclusively senses the MICH degree of freedom. Thus, the error signal extracted from the p-polarized field can be used to lock the MICH degree of freedom and, furthermore, it exhibits little sensitivity to perturbations in the other longitudinal DOF.

The simulations resulted in the following findings:

- The signal extraction ports in the optical setup were chosen with respect to optimal decoupling of all heterodyne length signals. Our preferred signal extraction port configuration is depicted in Fig. 2, further details are given in Tab. 1.
- For the general case of unequal lengths $L_{\text{SR1}} \neq L_{\text{SR2}}$ of the TSRC, the longitudinal degrees of freedom MICH and PRC showed strong coupling to the error signals for the SRM and TSRM positions.
- We found that in order to reduce the coupling of MICH and the SRM position to the TSRM error signal it was desirable to arrange for identical lengths in the TSRC, i.e. choosing $L_{\text{SR1}} = L_{\text{SR2}}$.
- Finally, from the optimized sensing matrix given in Tab. 2 we could deduce a suitable

order for the hierarchical locking of the interferometer. Lock acquisition starts with (i) the PRC, followed by (ii) MICH, (iii), the TSRM, and is completed with the stabilization of (iv) the SRM position.

Table 2. Normalized sensing matrix as obtained from the numerical model of the TSR interferometer. Rows correspond to different signal extraction ports, columns to different longitudinal DOF. For the calculation of each entry it was assumed implicitly that the other DOF were at their designated operating points. Heterodyne length signals which stem from unwanted coupling of neighboring DOF are highlighted in blue, numerical zeros are printed in green.

	PRC	MICH	δL_{SR2}	δL_{SR1}
PD _{PRC}	1	1.18×10^{-6}	0	0
PD _{MICH}	-9.32×10^{-4}	1	0	0
PD _{SR2}	-579.19	-32.18	1	-55.70
PD _{SR1}	-3.07	-0.12	8.18×10^{-3}	1

3. Experimental setup

We now proceed with a discussion of the optical setup of the interferometer, depicted in the schematic drawing in Fig. 3.

The main laser source was a Nd:YAG Innolight Mephisto NPRO laser with a nominal cw output power of 2 W at 1064 nm which was shared with adjacent experiments. Approximately 50% of the light was picked off and transmitted through a rigid, aluminum spacer-mounted ring cavity (“mode cleaner”) for spatial filtering and the suppression of high-frequency amplitude and phase noise of the laser beam. The PDH reflection locking technique [17] was employed to keep the mode cleaner cavity (MC) on resonance. Control sidebands were imprinted on the laser field by directing the beam through an electro-optic modulator (EOM) which was driven by an electronic oscillator at 18 MHz. Appropriate feedback signals were extracted by demodulating the field reflected by the MC, to obtain the 18 MHz beat signal of the PM sidebands with the carrier. A piezoelectric transducer (PZT), which was glued to one of the MC cavity mirrors, served as an actuator to tune the cavity length. The MC was locked by applying a high voltage (HV) amplified correction signal to the PZT, which was generated by servo electronics.

Prior to its injection into the interferometer the filtered laser beam was directed through two EOMs to imprint two pairs of PM control sidebands on the input field, at 15 MHz and at 123.6 MHz, respectively. The EOMs were followed by a Faraday isolator to attenuate back-reflected light from the interferometer and, in conjunction with a wave plate, to adjust the laser power at the interferometer input. Another two wave plates were placed between the isolator and the PRM: a quarter wave plate to eliminate elliptically polarized components of the input field and a half wave plate to adjust the linear polarization vector of the input beam. Together with the polarizing beam splitter (PBS) in the interferometer, between the main beam splitter (BS) and the SRM, this allows for independent sensing of the two polarization modes, thus providing an effective way to obtain a signal for MICH which exhibited nearly perfect decoupling from the position of the SRM (cf. Sec. 2.2). A number of lenses and steering mirrors in the input optics optical train served to match the input beam to the eigenmode of the PRC. For the investigations discussed in this paper the interferometer was illuminated with approximately 40 mW of input laser light, composed of 75% s-polarized and 25% p-polarized light.

The beam transmitted by the PRM, which had a power reflectivity of $R_{\text{PRM}} = 90\%$ and a ROC of 2 m, propagated towards the BS of the Michelson interferometer where it was split into

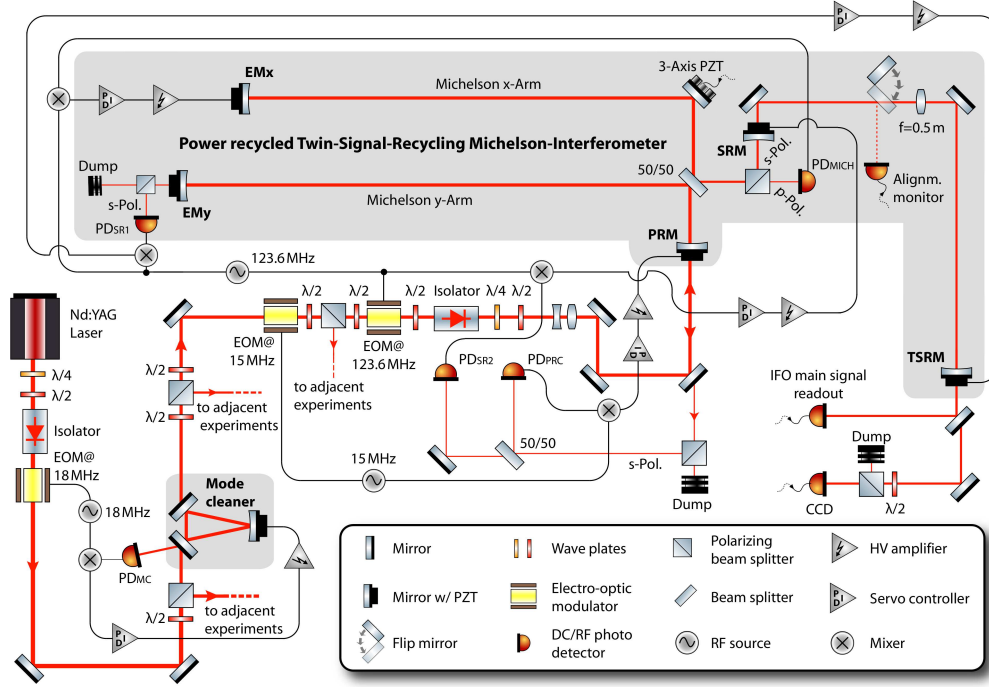


Fig. 3. Optical layout of the power recycled twin signal recycling interferometer experiment. A number of auxiliary optics were omitted for clarity.

two beams of equal power which then propagated along the parallel (due to space limitations) interferometer arms. The parallel arrangement of the arms required a steering mirror in the x-arm which was mounted in 3-axis piezo-driven mirror mount for easy “on-the-fly” tuning of the interferometer alignment. Both interferometer end mirrors (EMx, EMy) had a nominal ROC of 1.5 m and a power reflectivity of 99.92%. A Schnupp asymmetry of 7 mm was introduced to the Michelson arms to allow for control sideband leakage into the detection port while the interferometer was locked on the dark fringe [18].

The two recycling mirrors in the asymmetric port were placed at distances of 0.21 m (SRM) and 1.42 m (TSRM) from the Michelson BS, respectively, measured with respect to their reflective surfaces. Reflectivity and curvature of the SRM were 90% and 2 m, respectively. The plane TSRM was coated for a reflectivity of 95%. For the cavity formed by the SRM and the TSRM a convex-plane geometry was adopted, with an additional plano-convex intra-cavity lens with a focal length of 0.5 m. Due to its higher flexibility this configuration was preferred to a TSRM with custom-made ROC.

All five interferometer mirrors were mounted in 3-axis mounts, with a clamped PZT for actuation in the direction perpendicular to the mirror surface. The positions of the PRM, the SRM and the TSRM were actuated on by applying a HV signal to their respective PZT actuator. Actuation of the MICH degree of freedom was achieved by driving a PZT in one of the Michelson end mirror mounts.

Numerous photo detectors were employed to extract RF signals for length sensing as well as DC signals for diagnostics, e.g. to determine the quality of the alignment and mode matching of the experiment and for monitoring of the “state” of each of the longitudinal DOF (either locked or freely fluctuating). A CCD camera was placed in transmission of a steering mirror in the

detection port for online monitoring of the spatial shape of the beam leaving the interferometer. Furthermore a number of flip-mirrors were introduced in the setup, to pick off light internally for alignment and diagnostics purposes.

Due to the optical coupling of the Michelson interferometer with the recycling cavities it was a non-trivial task to bring the interferometer to a well-aligned state. To optimize the angular alignment and the mode matching of the interferometer, an iterative alignment scheme was developed. A necessary prerequisite was to “disable” the PRC prior to optimizing the Michelson fringe contrast and aligning the TSRC. This suppression of the PRC resonance was achieved by tilting the PRM. The slightly different optical path lengths of the tilted and the aligned PRM had no observable degrading effect on the final alignment quality.

Table 3. Design parameters of the power recycled TSR interferometer experiment.

Michelson arm length	1 m \pm 7 mm	Nominal ROC EMx, EMy	1.5 m
Distance of PRM/SRM to BS	0.21 m	Nominal ROC PRM/SRM	2 m
Distance SRM to TSRM (L_{SR1})	1.21 m	Nominal ROC TSRM	plane
Recycling cavity FSR	123.6 MHz	Intra-cavity lens focal length	0.5 m
Reflectivity EMx, EMy	99.92%	Beam waist size in PRC	499 μ m
Reflectivity PRM/SRM, TSRM	90%, 95%	Beam waist size on TSRM	181 μ m

4. Lock acquisition and measurements

In this section we discuss the aspect of bringing the aligned and mode matched, yet uncontrolled interferometer to a fully locked state of its four longitudinal DOF.

The hierarchic stabilization of the lengths in the interferometer was carried out in the order which was derived from the numerical interferometer model, as described in Sec. 2.2. Due to different types of imperfections, which inevitably occur in any real interferometer, the extracted heterodyne signals were likely to deviate from those obtained from the strongly idealized numerical model. Among these imperfections are e.g. non-ideal mode matching and the presence of higher-order modes, non-optimal demodulation phases, deviations from nominal lengths and also the coupling of length fluctuations from yet unstabilized DOF, which was not included in the model. Several iterations were necessary to optimize the relevant parameters and settings to fully lock the interferometer for the first time. In this stage of the experiment the CCD camera in the detection port helped to determine whether the interferometer was accidentally locked on some residual higher order mode or on the desired fundamental mode.

As a figure of merit, and also to document the transition of the interferometer from the initial, unlocked state to a fully locked final state, light powers in different optical ports along with the correction signals generated by the servo controllers were monitored during the acquisition phase and after lock was acquired. We used two digital storage oscilloscopes to record the data of two consecutive exemplary measurements which we present in Figs. 4 and 5.

The shaded regions in the plots represent different stages of the lock acquisition process:

1. All DOF unlocked, mirror positions randomly fluctuating.
2. MICH manually tuned close to the dark fringe, PRC length locked (red traces).
3. MICH locked on the dark fringe using p-polarized light (green traces).
4. The TSRM position was scanned by applying a triangular drive to its PZT. The SRM was tuned manually to its operating point to obtain a decent error signal for feedback to the TSRM, to lock δL_{SR1} (yellow traces).

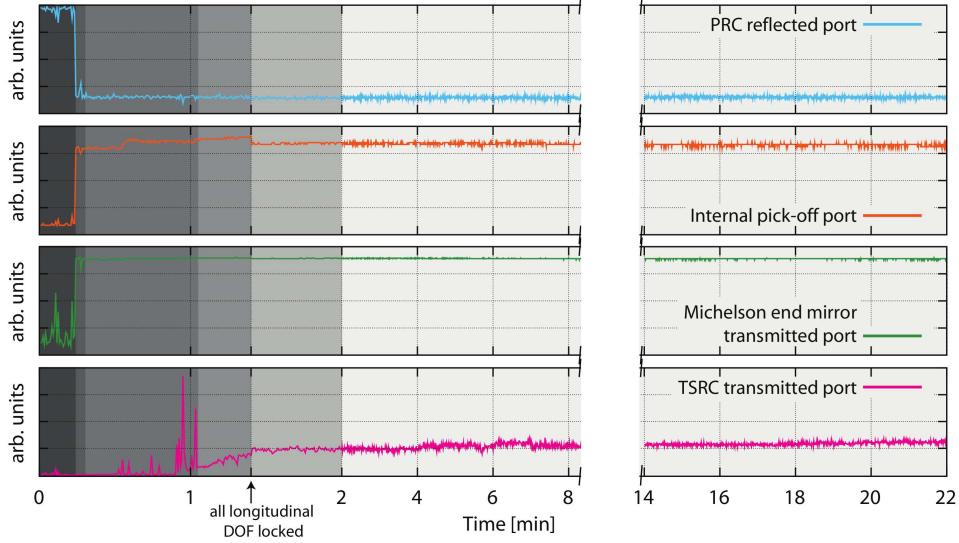


Fig. 4. Monitored photo detector DC transients, recorded during lock acquisition and fully locked operation of the interferometer. The traces show light powers measured in the symmetric port (i.e. in reflection of the power recycling cavity, blue trace), in the Michelson-internal pick-off port (orange trace), in the port in transmission one of the Michelson end mirrors (green trace) and in the asymmetric port (i.e. in transmission of the TSRC, magenta trace). The grey shaded areas represent different stages of the acquisition sequence, resulting in a fully locked interferometer after $t = 1.4$ min. The proportional gains of the feedback loops were optimized for long-term stable operation at $t = 2$ min.

5. The position of SRM stabilized to its designated operating point, δL_{SR2} locked (blue traces).
6. All longitudinal DOF are electronically stabilized. Proportional gains of the servo loops adjusted to optimize loop suppression.

In Fig. 5, when δL_{SR2} lock is acquired at 1.4 minutes, we can observe a correlated jump in the SRM and TSRM correction signals. This is due to the attempt of the TSRM servo to maintain the operating point for δL_{SR1} , i.e. the servo commands the TSRM to swiftly follow the SRM when the SRM position is locked.

The p-polarization-based probing of the MICH degree of freedom gave rise to a small amount of s-polarized light leaking out of the asymmetric port. This is due to a non-degeneracy of s- and p- polarized light with respect to covered optical path lengths in the interferometer and resulted in a slight offset of the Michelson operating point from the dark fringe for the s-polarized field.

Special care needed to be taken to prevent oscillations to occur in the servo controllers during acquisition. Due to mutual dependencies of the control loops, a consequence of the coupling of the longitudinal DOF, the proportional gains of the servo controllers needed to be set carefully, to thoroughly balance the suppression of disturbances that would cause immediate lock-loss versus loop instability. We also found that slightly tuning the higher sideband frequency improved the robustness of our locking scheme. This could be attributed to small deviations of the recycling cavity lengths from their nominal values.

Our optimizations of the experiment led to a gradual increase of the time the interferometer remained in a fully locked state of up to tens of minutes. The limited duration of the locks could be explained by long-term drifts in the longitudinal DOF of the interferometer, e.g. due to

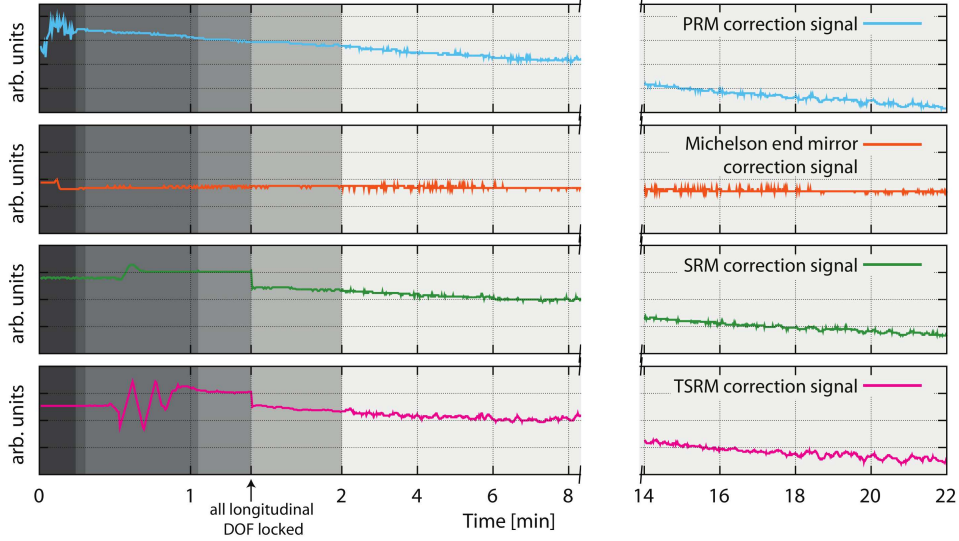


Fig. 5. Monitored correction signals generated by the servo controllers for the four longitudinal DOF. The traces were recorded simultaneously with the data shown in Fig. 4. These signals were amplified and in turn applied to piezoelectric transducers actuating on the power recycling mirror (blue trace), one of the Michelson end mirrors (orange trace), the signal recycling (green trace) and the twin signal recycling mirror (magenta trace), respectively. Long term drifts eventually led to a lock-loss of the instrument due to the limited range of the actuators.

thermal expansion of components in the setup but also due to drifts of the input laser frequency. Drifts exceeding the range of the PZT actuators eventually led to lock-loss of the interferometer. In the example shown in Fig. 4 and Fig. 5, lock of all four longitudinal DOF was acquired 1.4 minutes after the measurement started and lasted for more than 20 minutes until the actuator range of the PRM was exceeded.

A significant improvement of the duty cycle could be expected from operating the interferometer in vacuum. This was, however, not within the scope of the experiment described here.

5. Conclusion and outlook

In this paper we described the design, the implementation and the successful operation of a laboratory-scale power recycled Michelson interferometer with twin signal recycling.

With the aid of numerical simulations we derived a length sensing and control scheme which we successfully applied to the experiment, to stably lock the interferometer in its four longitudinal degrees of freedom. After a series of iterative optimizations we were able to operate the fully locked interferometer on time scales of tens of minutes, limited by long-term drifts in the optical setup exceeding the range of the actuators.

Based on the setup discussed in this paper, the aspect of squeezing injection into a twin signal recycling interferometer was investigated in a subsequent experiment. Results of this work were already published in [12].

Future work will include the transfer of the twin signal recycling technique to other detector topologies, e.g. Michelson interferometers with Fabry-Perot arm cavities, which will form the basis of all second generation as well as the planned third generation observatories, e.g. the Einstein Telescope [19].

Acknowledgements

This work has been supported by the International Max Planck Research School (IMPRS) and the cluster of excellence QUEST (Centre for Quantum Engineering and Space-Time Research).